Supporting Information

Impact of trace extrinsic defect formation on the symmetry transition in spinel $LiNi_{0.5}Mn_{1.5}O_{4-\delta}$ and their electrochemical characteristics

Hiromasa Shiiba,[a,‡] Nobuyuki Zettsu, [a,b,‡,*] Satoru Kida,[a] Dae-wook Kim,[a] and Katsuya Teshima [a,b,*]

[a] Department of Materials Chemistry, Shinshu University, 4-17-1 Wakasato, Nagano 380-8553, Japan

[b] Center for Energy and Environmental Science, Shinshu University, 4-17-1 Wakasato, Nagano 380-8553, Japan

A schematic illustration of the metal excess model is shown in Fig. S1. The defect formation energy in metal excess models is expressed with Kröger-Vink;

$$\frac{1}{4}\left(LiNi_{0.5-x}Mn_{1.5}M_xO_4\right) \rightarrow \frac{1}{4}\left(Li_i^{\cdot} + \left(\frac{1}{2}-x\right)Ni_i^{\cdot\cdot} + \frac{3}{2}Mn_i^{\cdot\cdot\cdot\cdot} + xM_i^{\cdot\cdot} + 8e^{'} + 2O_2\right) \quad \text{(S1)}$$

$$\frac{1}{4}\left(LiNi_{0.5}Mn_{1.5-y}M_yO_4\right) \rightarrow \frac{1}{4}\left(Li_i^{\cdot} + \frac{1}{2}Ni_i^{\cdot\cdot} + \left(\frac{3}{2}-y\right)Mn_i^{\cdot\cdot\cdot\cdot} + yM_i^{\cdot\cdot\cdot\cdot} + 8e^{'} + 2O_2\right) \quad \text{(S2)}$$

The defect generation energy can be expressed with the equations (1) and (2) in the main text using the total energy E (X) obtained by the first principles calculation.

Effects of transition metal substitution on the Ni^{2+}/Mn^{4+} ordering

Two different types of oxygen defect models, an oxygen vacancy model and metal-excess model, were used for the calculations. Oxygen vacancies occupied at nearest neighbor oxygen sites from substituted metals in the oxygen vacancy model. The oxygen vacancy formation energies for $P4_332$ and $Fd\text{-}3m$ $LiNi_{0.375}Mn_{1.5}M_{0.125}O_4$ and $LiNi_{0.5}Mn_{1.375}M_{0.125}O_4$ (M = Ti, V, Cr, Fe, Co, Cu, Zn, Sn) are summarized in Supplementary Figure S1. From the crystallographic features, oxygen atoms included in both $P4_332$ and $Fd\text{-}3m$ type symmetries have two possible spatial

configurations: coordinated with one Ni atom and two Mn atoms, or coordinated with three Mn atoms. A series of $LiNi_{0.375}Mn_{1.5}M_{0.125}O_4$ derivatives showed higher formation energies than those of $LiNi_{0.5}Mn_{1.375}M_{0.125}O_4$ compounds independent of the transition metal type. Since the formation of lattice defects as described by M_{Ni2+} simultaneously generates Mn^{3+} and M_{Mn4+} lattice defects due to corresponding charge neutralization, oxygen vacancy-free $LiNi_{0.375}Mn_{1.5}M_{0.125}O_4$ compounds are considered to be less stable. In contrast, the oxygen vacancy formation energies for the incorporation of Fe_{Mn}, Cu_{Ni}, Cu_{Mn}, and Zn_{Mn}, were significantly lower than stoichiometric $LiNi_{0.5}Mn_{1.5}O_4$. In particularly, divalent Cu_{Mn}^{2+} and Zn_{Mn}^{2+} can be preferentially incorporated at oxygen vacancy sites without Mn^{3+} formation.

We further considered the effects of Frenkel defects, in which transition metals occupy interstitial sites, by using the metal-excess model for DFT calculations. The positions of two neighboring tetrahedral Li ions are assumed to migrate to octahedral vacancy sites, as shown in Supplementary Figure S2(a); this is the most stable cationic arrangement for interstitial Ni and Mn. Defect formation energies for the metal-excess model for $LiNi_{0.5-x}Mn_{1.5}M_xO_4$ and $LiNi_{0.5}Mn_{1.5-y}M_yO_4$ ($0 \leq x \leq 0.125$, $0 \leq y \leq 0.125$, M = (b) Ti, (c) V, (d) Cr, (e) Fe, (f) Co, (g) Cu, (h) Zn, (i) Sn) with $P4_332$ and *Fd*-3*m* type symmetries were summarized in Supplementary Figure S2(b-i). As in the case of the stoichiometric $LiNi_{0.5}Mn_{1.5}O_4$, the defect formation energy of the *Fd*-3*m* type structure was lower than that of the $P4_332$ structure, independent of the transition metal cation inducing the extrinsic defect formation. We further evaluated antisite defect formation energies for the substituted transition metals and neighboring Ni/Mn in both $P4_332$ and *Fd*-3*m*, as shown in Supplementary Figure S3. The Ni or Mn sites forming the antisite defects are spatially distinguished by the difference in the point-to-point sharing and the edge sharing with the Li octahedron. Two different Ni sites (P - MNi

1, P - MNi 2) and two Mn sites (P - MMn 1, P - MMn 2) are possible in the $P4_332$ structure, and one possible Ni site (F - MNi) and three Mn sites (F - MMn 1, F - MMn 2, F - MMn 3) exists in the *Fd*-3*m* structure, respectively. Our calculations imply that Ti, V, Cr, Fe, Co, Sn cations preferentially occupy Mn sites, forming extrinsic defects ($Ti_{Mn}^{\times}$, $V_{Mn}^{\times}$, $Cr_{Mn}^{'}$, $Fe_{Mn}^{'}$, $Co_{Mn}^{'}$, $Sn_{Mn}^{\times}$) compared to the occupation of interstitial sites (Frenkel defects). In contrast, Cu^{2+} favorably occupied interstitial sites ($Cu_{int}^{\cdot\cdot}$). We estimated the energy for disordering Ni/Mn arrangements caused by the penetration of transition metals into interstitial sites (Supplementary Figure S4). This implies that the Ni/Mn disordering was highly promoted due solely to Cu substitution according to negative antisite energy.

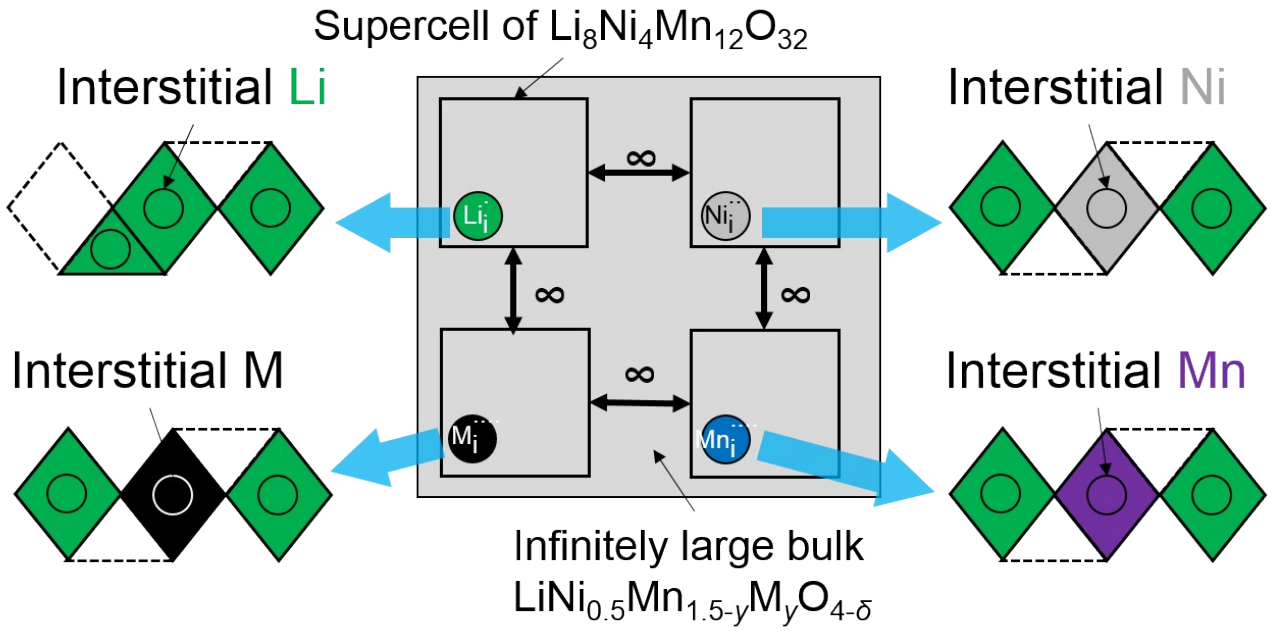

Supplementary Figure S1

Schematic illustration of metal-excess model for $LiNi_{0.5}Mn_{1.5-y}M_yO_4$.

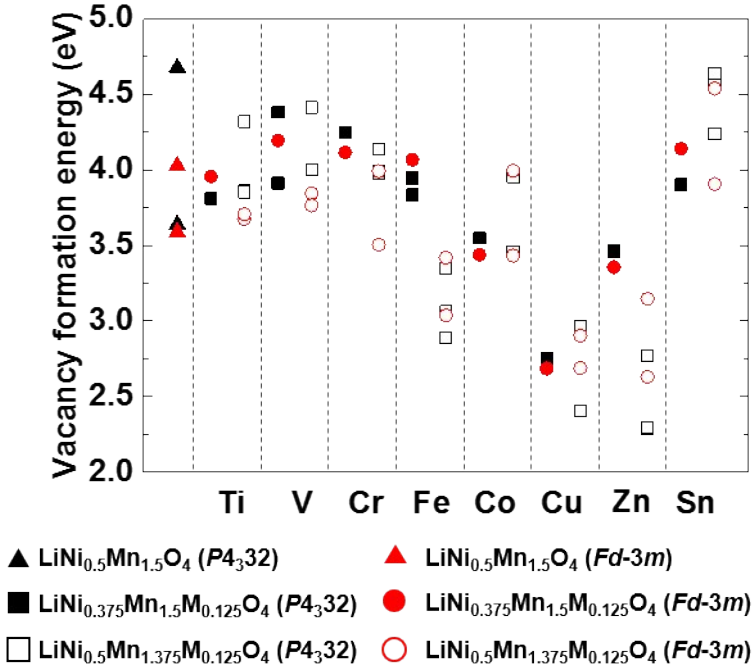

Supplementary Figure S2

Oxygen vacancy formation energies for stoichiometric $LiNi_{0.5}Mn_{1.5}O_4$ with $P4_332$ and Fd-3m type symmetries.

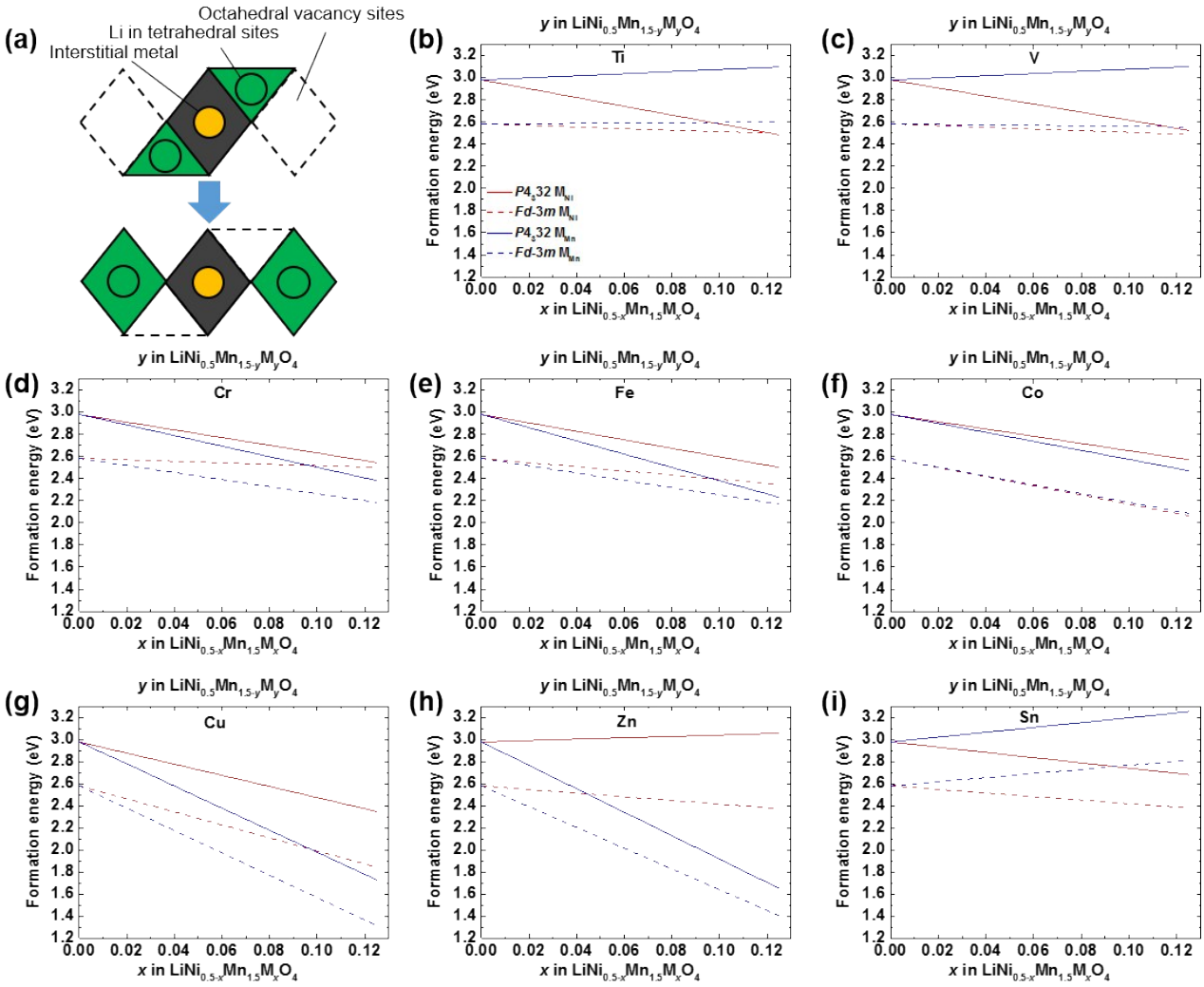

Supplementary Figure S3

(a) Schematic illustration of positional transitions in two neighboring tetrahedral Li ions to octahedral vacancy sites, and defect formation energies for metal-excess model for $LiNi_{0.5-x}Mn_{1.5}M_xO_4$ and $LiNi_{0.5}Mn_{1.5-y}M_yO_4$ ($0 \le x \le 0.125$, $0 \le y \le 0.125$, M = (b) Ti, (c) V, (d) Cr, (e) Fe, (f) Co, (g) Cu, (h) Zn, (i) Sn) with $P4_332$ and Fd-3m type symmetries.

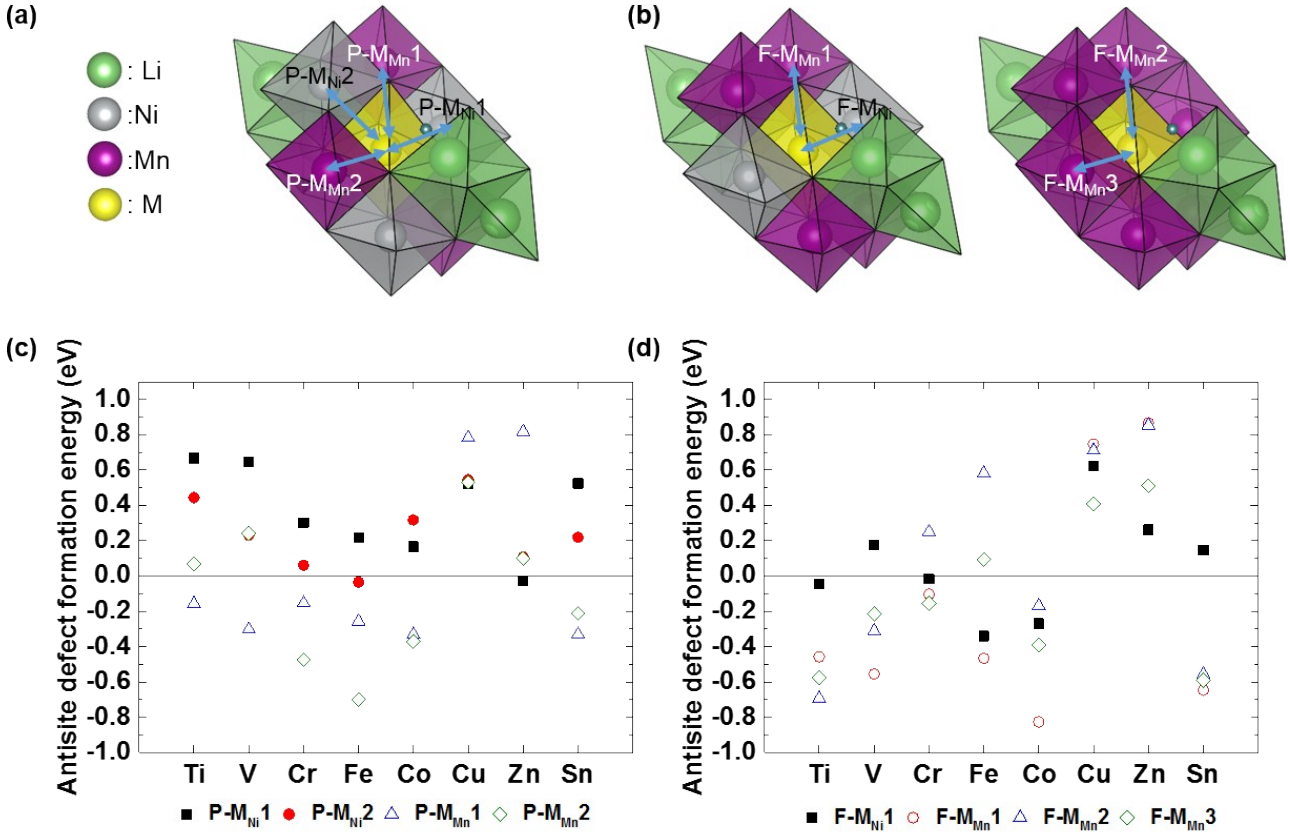

Supplementary Figure S4

Atomic arrangement of nearest neighbor (NN) Ni/Mn around incorporated extrinsic interstitial metal (a) in $P4_332$, and (b), (c) in *Fd*-3*m* type structures. Possible antisite defects for the interstitial metal and NN Ni/Mn are described in the illustrations by the arrows. Corresponding antisite defect formation energies in both (d) $P4_332$ and (e) *Fd*-3*m*

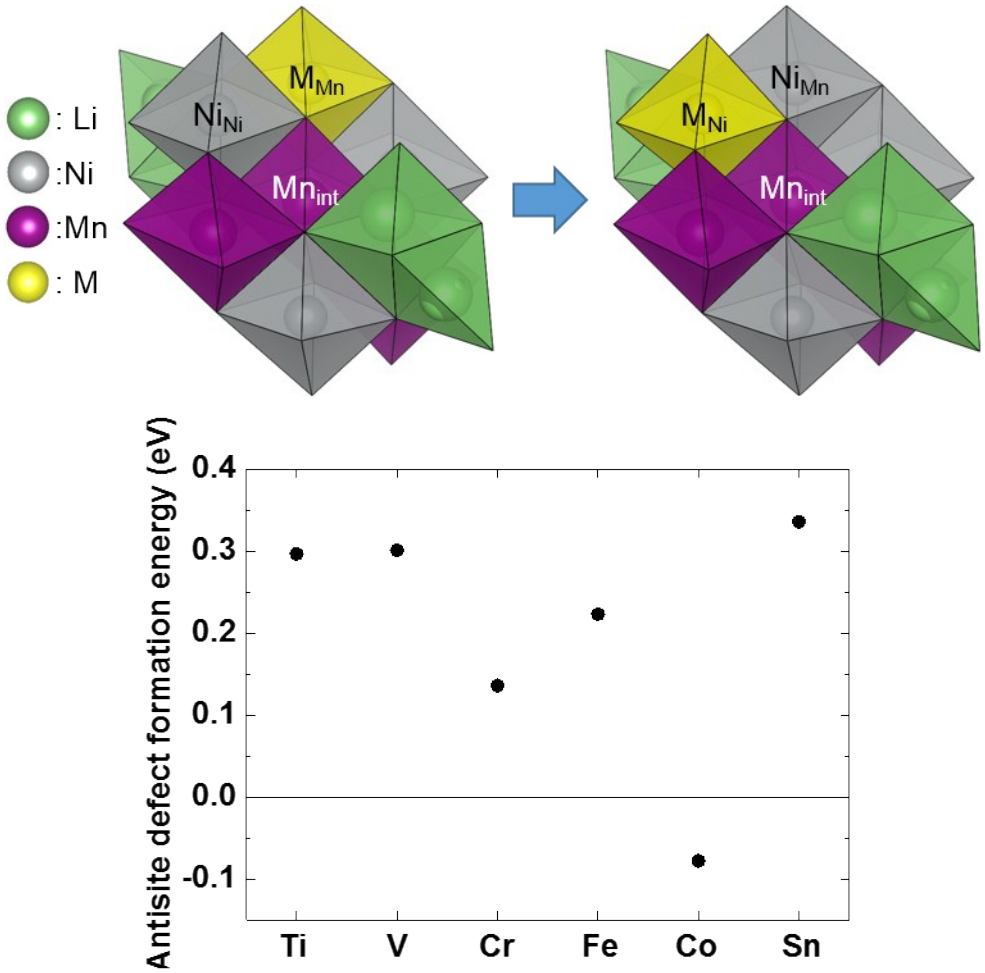

Supplementary Figure S5

Antisite defect formation energies for the substituted transition metal and neighboring Ni in $LiNi_{0.5}Mn_{1.5}O_4$ with $P4_332$ symmetry

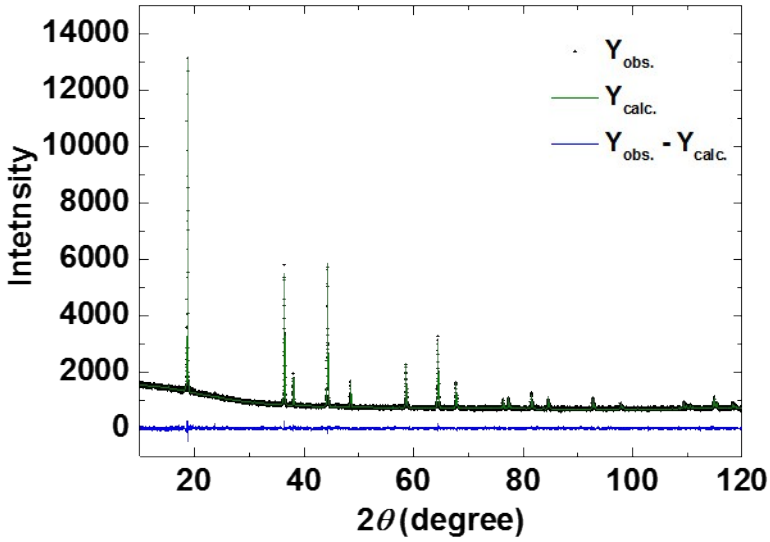

Site	Atom	*x*	*y*	*z*	*g*	*B*
8c	Li	0.000(8)	0.000(-)	0.000(-)	1(-)	1(-)
4a	Ni	0.625	0.625	0.625	1.0(-)	1.1(4)
	Cu1				0.009(-)	
12d	Mn	0.125	0.3709(8)	0.8791(-)	1.0(1)	0.5(1)
	Cu2				0.005(-)	
8c	O1	0.393(3)	0.393(-)	0.393(-)	1(-)	0.3(-)
24e	O2	0.130(3)	0.865(2)	0.142(3)	0.87(2)	0.3(1)

R_{wp} = 3.403%, R_p = 2.692%, R_e = 3.395%, S = 1.003, a = 8.1691(1) Å

Supplementary Figure S6

Powder XRD profiles and Rietveld refinement results of the Cu-incorporated $LiNi_{0.5}Mn_{1.5}O_{4-\delta}$ derivative crystals.

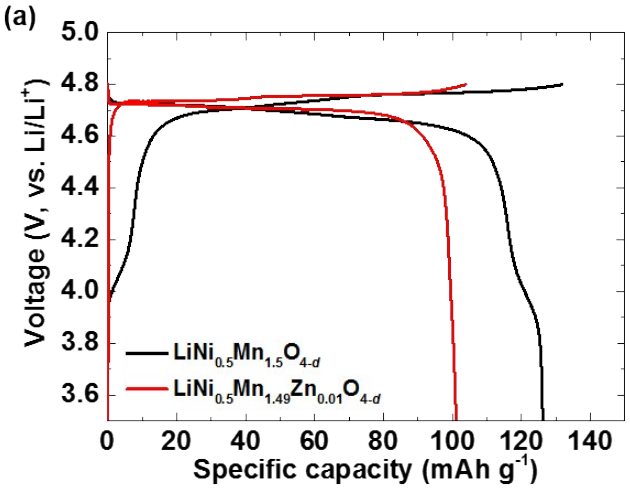

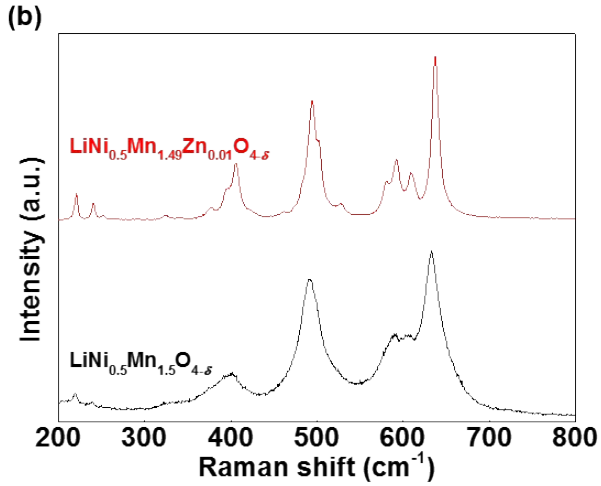

(c)

	Li/M antisite energy (eV)
Cu	0.99
Zn	0.05

Supplementary Figure S7

(a) Third cycle charge–discharge profiles at a current density corresponding to 0.2 C at room temperature of $LiNi_{0.5}Mn_{1.5}O_{4-\delta}$/Li and $LiNi_{0.5}Zn_{0.01}Mn_{1.49}O_{4-\delta}$/Li cells. (b) Raman shift of $LiNi_{0.5}Mn_{1.5}O_{4-\delta}$ and $LiNi_{0.5}Mn_{1.49}Zn_{0.01}O_{4-\delta}$. (c) The calculated Li/M Antisite defect formation energies of $LiNi_{0.5}Mn_{1.5}O_{4-\delta}$ and $LiNi_{0.5}Mn_{1.49}Zn_{0.01}O_{4-\delta}$.

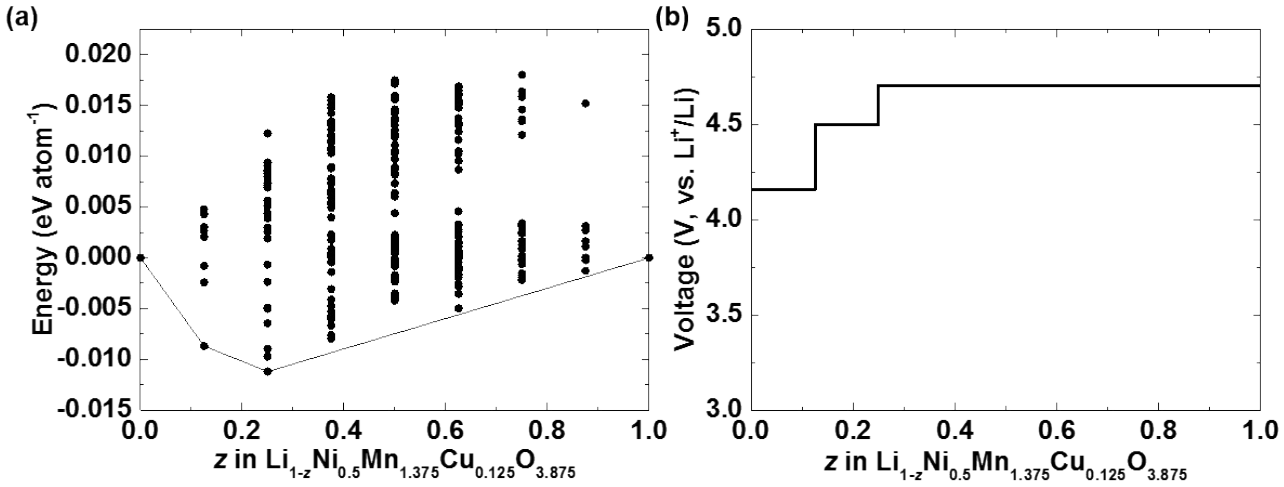

Supplementary Figure S8

(a) Formation energies for the most stable Li/vacancy arrangement and (b) theoretical voltage slope as a function of z in $Li_{1-z}Ni_{0.5}Mn_{1.375}Cu_{0.125}O_{3.875}$.

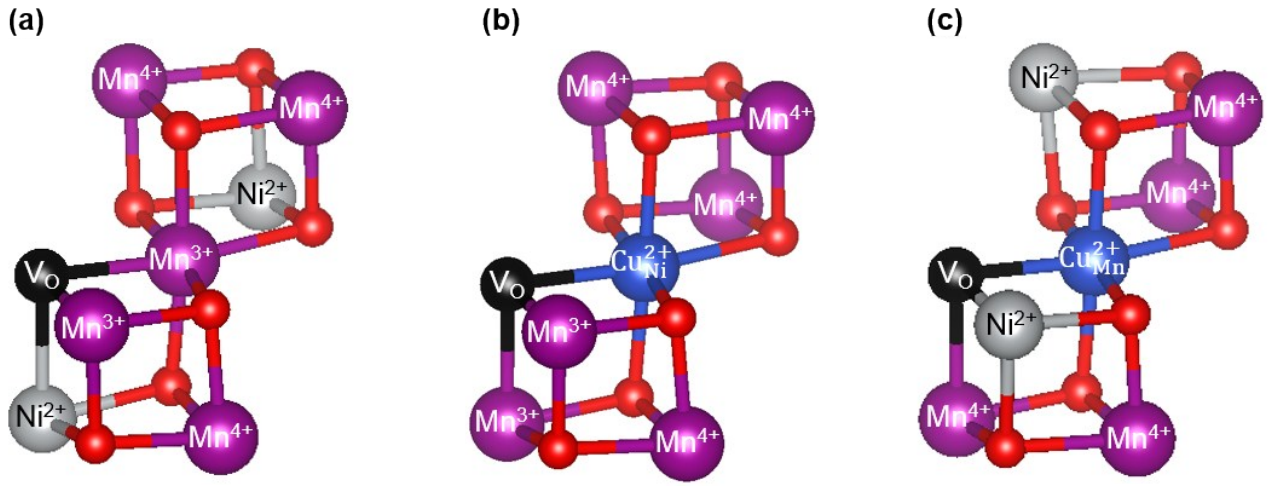

Supplementary Figure S9

Atomic valence distribution near the Cu^{2+} and oxygen vacancies in (a) $LiNi_{0.5}Mn_{1.5}O_{4-\delta}$, (b) $LiNi_{0.5-x}Mn_{1.5}Cu_xO_{4-x}$, and (c) $LiNi_{0.5}Mn_{1.5-y}Cu_yO_{4-y}$.

Supplementary Table S1

Chemical compositions of $LiNi_{0.5}Mn_{1.5}O_{4-\delta}$ and Cu-incorporated derivative crystals, as evaluated by inductively coupled plasma optical emission spectrometry.

	Li	:	Ni	:	Cu	:	Mn
Cu-incorporated $LiNi_{0.5}Mn_{1.5}O_{4-\delta}$	1.98	:	1	:	0.02	:	2.98
$LiNi_{0.5}Mn_{1.5}O_{4-\delta}$	1.96	:	1	:	-	:	3.02